Journal of Alloys and Compounds 875 (2021) 159987

Contents lists available at ScienceDirect

Journal of Alloys and Compounds

journal homepage: www.elsevier.com/locate/jalcom

Highly efficient field emission properties of vertically aligned 2D CuSe nanosheets: An experimental and theoretical investigation

Chandradip D. Jadhav[a,b,1], Sachin R. Rondiya[c,1], Reshma C. Hambire[a], Devashri R. Baviskar[a], Avinash V. Deore[d,e], Russell W. Cross[c], Nelson Y. Dzade[c], Padmakar G. Chavan[a,*]

[a] Department of Physics, School of Physical Sciences, Kavayitri Bahinabai Chaudhari North Maharashtra University, Jalgaon 425001, India
[b] The State Key Laboratory of Refractories and Metallurgy, Institute of Advanced Materials and Nanotechnology, College of Materials and Metallurgy, Wuhan University of Science and Technology, Wuhan 430081, PR China
[c] School of Chemistry, Cardiff University, Main Building, Park Place, Cardiff, CF10 3AT Wales, UK
[d] Springer Nature Technology and Publishing Solutions, Pune 411013, India
[e] Department of Physics, S. P. Pune University, Pune 411007, India

ARTICLE INFO

Article history:
Received 3 December 2020
Received in revised form 10 April 2021
Accepted 12 April 2021
Available online 19 April 2021

Keywords:
Chronoampereometry
Vertically aligned 2D CuSe nanosheets
Field emission
DFT

ABSTRACT

We report the synthesis of klockmannite (CuSe) via a three-probe electrochemical set-up (chronoampereometry). The structural properties are examined by X-ray diffraction and Raman spectroscopy. Field emission scanning electron microscopy (FESEM) analysis revealed the formation of vertically aligned CuSe nanosheets with an average thickness of 34 nm and an average lateral size of 700 nm. The CuSe nanosheets exhibit impressive field electron emission characteristics with a turn-on field of 1.4 V/μm for 10 μA/cm^2 emission current density. Also, a high current density of 5.8 mA/cm^2 is observed at a relatively low applied field of 3.1 V/μm. Complementary first-principles DFT calculations show that CuSe displays metallic conductivity, and the (001) surface has a low work function of 5.12 eV, which is believed to be responsible for the impressive field emission characteristics.

1. Introduction

In comparison with bulk materials, nanomaterials are popular for phase engineering as different phases of nanomaterials can be tuned with synthesis parameters for optimal performance [1,2]. The precise control over the synthesis of unconventional phases of nanomaterials has opened the door for various correlation studies between a structure, properties and appropriate applications. Rather than a routine study of core structures of nanomaterials and their applications in recent decades, many structural developments/modifications in nanomaterials have been carried out for particular applications such as magnetic [3], electronic [4], mechanical [5], catalytic [6], and optical devices [7].

In line with the aforesaid structural developments, copper selenide (CuSe) has proved to have extraordinary properties for application in electronic and optoelectronic devices [8–10]. Copper selenide is found in a variety of stoichiometric compositions such as CuSe, Cu_3Se_2, Cu_2Se, Cu_2Se, Cu_5Se_4, Cu_7Se_4 and the non-stoichiometric $Cu_{2-x}Se$ [11–14]. Various synthesis techniques have been explored for the synthesis of CuSe nanomaterials including the chemical aqueous route [15], hydrothermal method [16], solvothermal method [17] and hot injection method [18]. However, reports on the synthesis of CuSe in the klockmannite phase are rather limited [19]. CuSe is popularly known for various potential applications such as photo-detectors [20], Shottky-diodes [21], solar cells [22] and field emission (Cu_{1-x} Se) [23].

Field electron emission is the fundamental process of electron ejection from a material surface which occurs under the application of a high electric field [24]. Field electron emission capabilities of various one-dimensional (1D) and two-dimensional (2D) nanomaterials have been explored in previous reports [25–31]. In particular, the 2D nanomaterials have been demonstrated to exhibit superior field emission properties in terms of turn-on field, high current density and emission stability [27]. Although CuSe has been studied for electronic and optoelectronic applications, the suitability of 2D CuSe nanosheets for field emission applications has not been investigated thoroughly.

Herein, we report a simple one-pot synthesis of vertically aligned, single crystalline, 2D CuSe nanosheets and subsequent field emission characteristics. In addition, theoretical investigation of the electronic structure and work function of CuSe have been carried out using first-principles density functional theory calculations.

* Corresponding author.
E-mail address: pgchavan@nmu.ac.in (P.G. Chavan).
[1] Authors equally contributed.

https://doi.org/10.1016/j.jallcom.2021.159987
0925-8388/

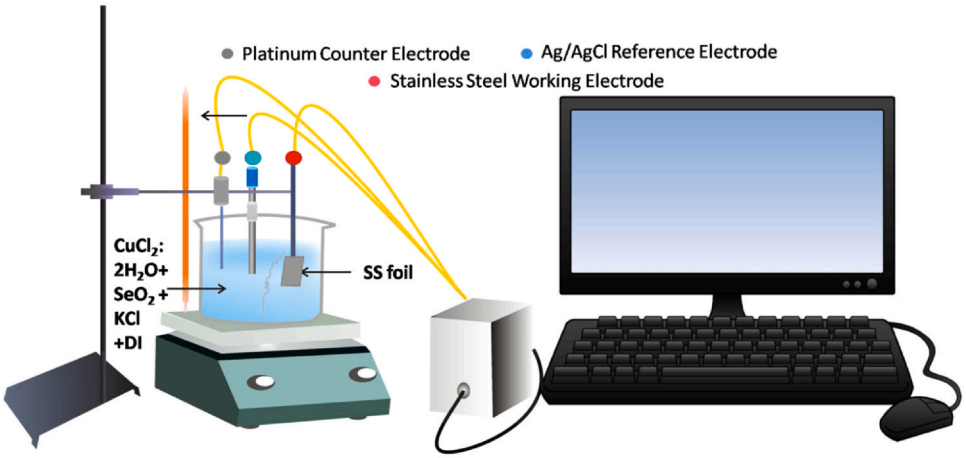

Fig. 1. Schematic for the synthesis of vertically aligned 2D CuSe nanosheets.

2. Experimental and characterizations

2.1. Synthesis

The synthesis of vertically aligned 2D CuSe nanosheets is done using a chronoampereometry technique. Fig. 1 shows a schematic of the experimental synthesis set-up. Stainless steel (SS) foil is used as the substrate throughout. $CuCl_2$:$2H_2O$ (2 mM), SeO_2 (4.5 mM) and KCl (0.1 mM) are combined in distilled water to make the electrolyte solution. 0.2 M HCl was added to adjust the electrolyte pH to 1.5. For the three-probe electrode system, SS foil, platinum (Pt) and calomel electrode (SCE) were used as the working, counter and reference electrodes, respectively. The vertically aligned 2D CuSe nanosheets were prepared via a potentiostatic approach. At the time of deposition, the applied potential was −0.15 *V* (vs SCE) and the temperature was kept constant at 60 °C for 30 min.

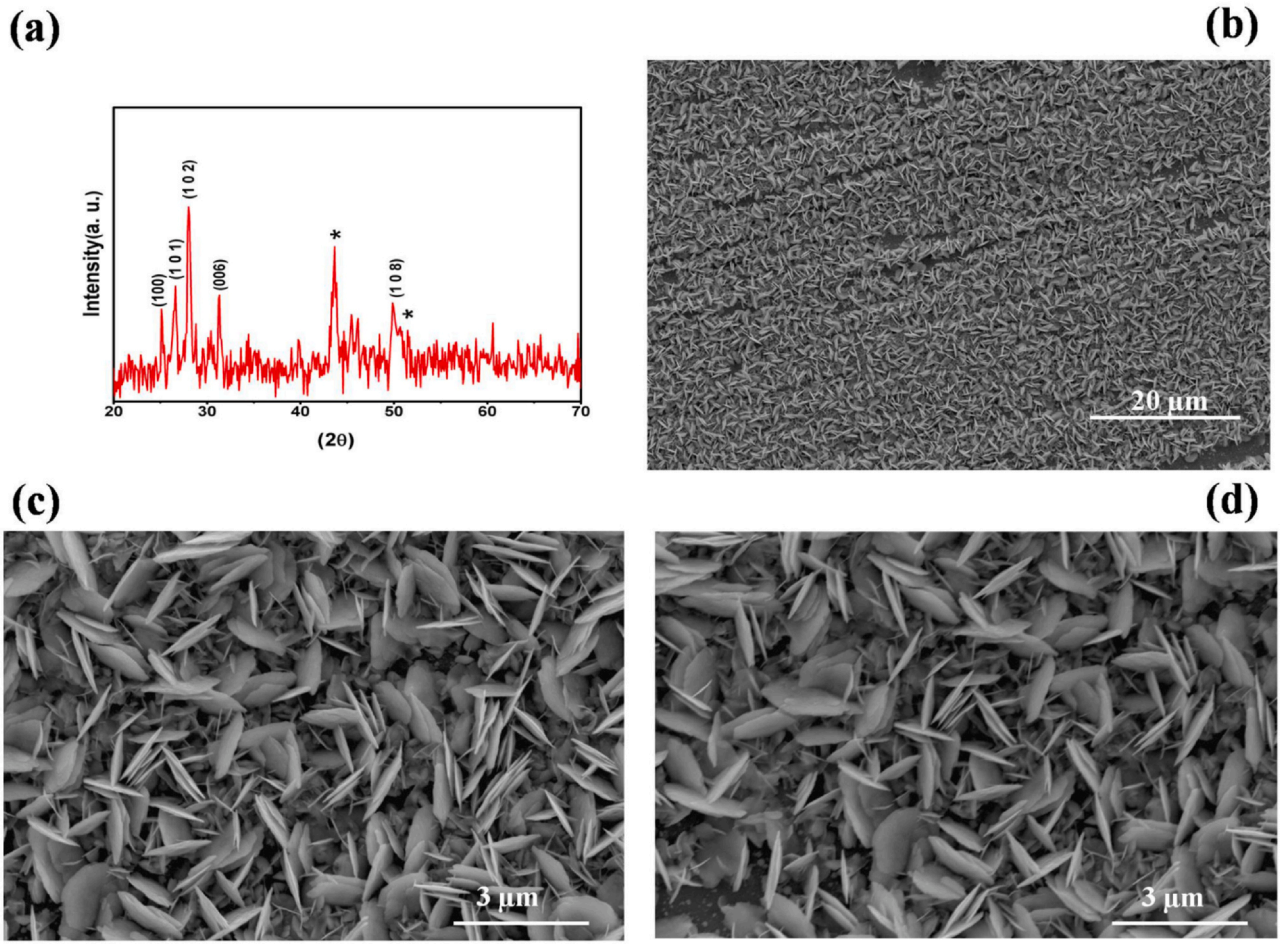

Fig. 2. (a) X-ray diffraction spectrum for klockmannite CuSe, (b–d)vertically aligned 2D CuSe nanosheets.

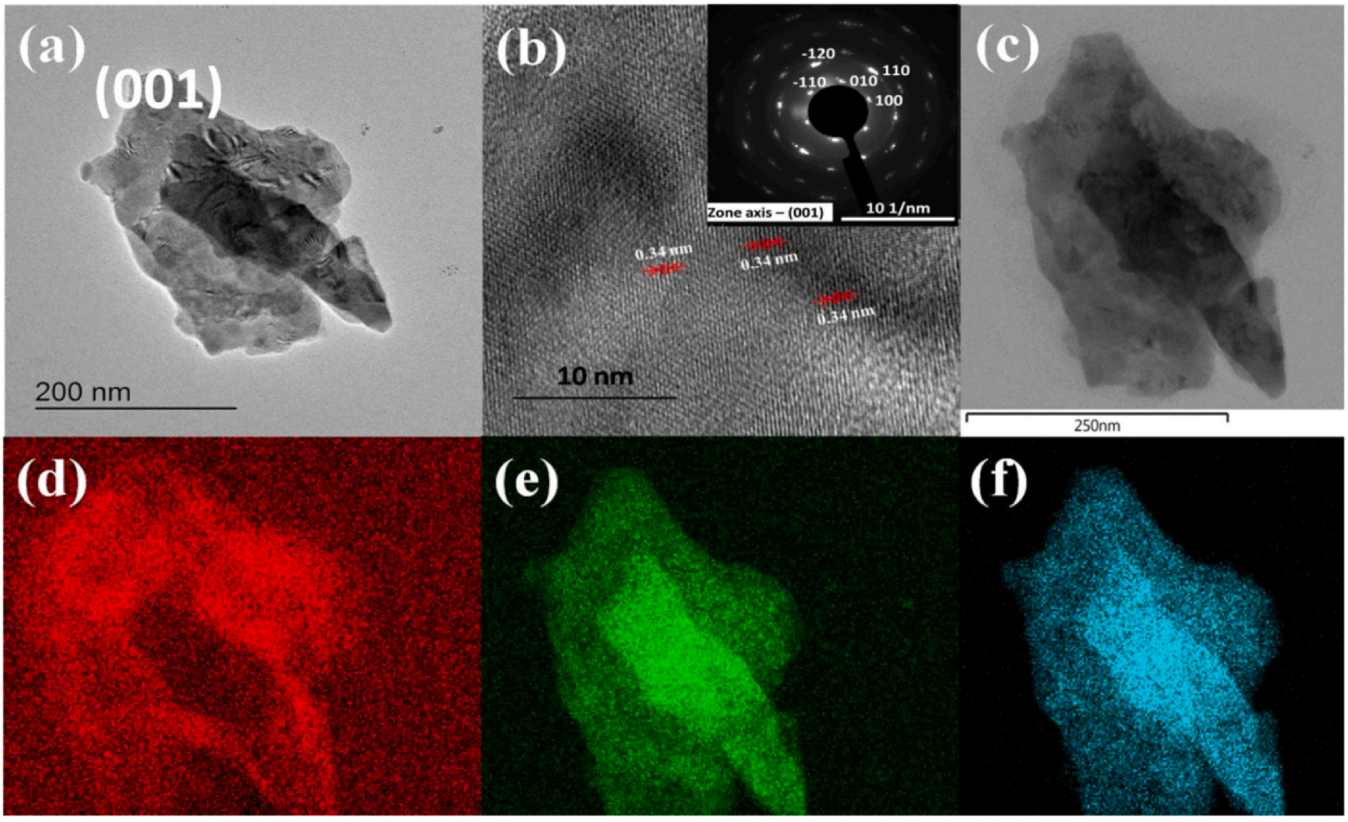

Fig. 3. (a) TEM image, (b) HRTEM image with fringe spacing and inset SAED pattern, (c) bright TEM image for elemental mapping, (d–f) elemental mapping images for C, Cu and Se elements with colors red, green and blue respectively. (For interpretation of the references to color in this figure legend, the reader is referred to the web version of this article.)

2.2. Materials characterization

X-ray diffraction studies were carried out by Bruker (D8 Advance) for a scan rate of 1°/min. A Field Emission Scanning Electron Microscope (FESEM) model-Quantum 450 FEG was used to examine the morphology and surface topography of the vertically aligned 2D CuSe nanosheets. The morphology and crystallinity of the as-prepared samples were studied by Transmission Electron Microscope (TEM), High Resolution Transmission Electron Microscope (HR-TEM) and Selected Area Electron Diffraction (SAED) (model number-JEOL 2200 FS, source-FEG 200 kV). Elemental mapping analysis was done using Energy-dispersive X-ray spectroscopy (EDS). The samples were dry dispersed over 300 mesh copper grids coated with holey carbon film. Field emission measurements such as the log of current density-applied field (log(*J*)-*E*) and current-time (*I*-*t*) were carried out at stable pressure ~1×10^{-8} mbar. The planer diode i.e., 'close proximity' configuration was employed during field emission studies [32]. In the present case, the area of CuSe specimen was 0.25 cm^2 and the separation between the anode and cathode was 1 mm. Here, the vertically aligned 2D CuSe nanosheets film was directly pasted onto sample holder using a highly conducting carbon tape. Ultra-high vacuum (UHV) was achieved with the help of turbo molecular pump and rotary pump. Above mentioned pressure (~1×10^{-8} mbar) reached after baking the system at 150 °C for 12 h. Here, the applied electric field is, $E = \frac{V}{d}$, where V is applied voltage and d is distance separated by anode and cathode.

2.3. Computational details

The density functional theory (DFT) calculations were performed using the Vienna Ab initio Simulation Package (VASP) [33–35], a periodic plane-wave DFT code. The interactions between the core and valence electrons was described using the Project Augmented Wave (PAW) method [36]. A plane-wave basis set with a kinetic energy cut-off of 500 eV was used to converge the total energy of CuSe to within 10^{-6} eV. The Brillouin zone of bulk CuSe was sampled using a 7 × 7 × 3 Monkhorst-Pack *k*-point mesh [33]. All calculations were deemed to be converged when the forces on all atoms reached 0.001 eV/Å. The electronic exchange–correlation potential was calculated using the Perdew–Burke–Ernzerhof (PBE) generalized gradient approximation (GGA) functional [34]. The electronic structure (total and projected density of states) was determined using the screened hybrid functional HSE06 ($\alpha = 0.25$ and $\omega = 0.11$ $bohr^{-1}$) [35]. The most stable CuSe(001) surface has been used to characterize the work function of CuSe. Previous theoretical calculations have predicted the lowest surface energy for the (001) surface of CuS, which is isostructural to CuSe [37,38]. In order to align the energies to the vacuum level, a slab-gap model (slab thickness of 17.259 Å and vacuum size of 20 Å) was constructed and the corresponding electrostatic potential was averaged along the *c*-direction, using the Macro Density package [39–41]. The work function (Φ) was calculated as $\Phi = V_{vacuum} - E_F$, where V_{vacuum} and E_F are the vacuum and Fermi level, respectively.

3. Results and discussion

3.1. Structural properties

The X-ray diffraction spectrum of the vertically aligned 2D CuSe nanosheets is shown in Fig. 2a. The peaks observed at 25.11°, 26.61°, 28.01°, 31.32º and 49.86° can be indexed to CuSe klockmannite phase, with JCPDS card number #34-0171. The other peaks correspond to the SS substrate and are indexed by *. These peaks originate from C and Fe elements [42,43].

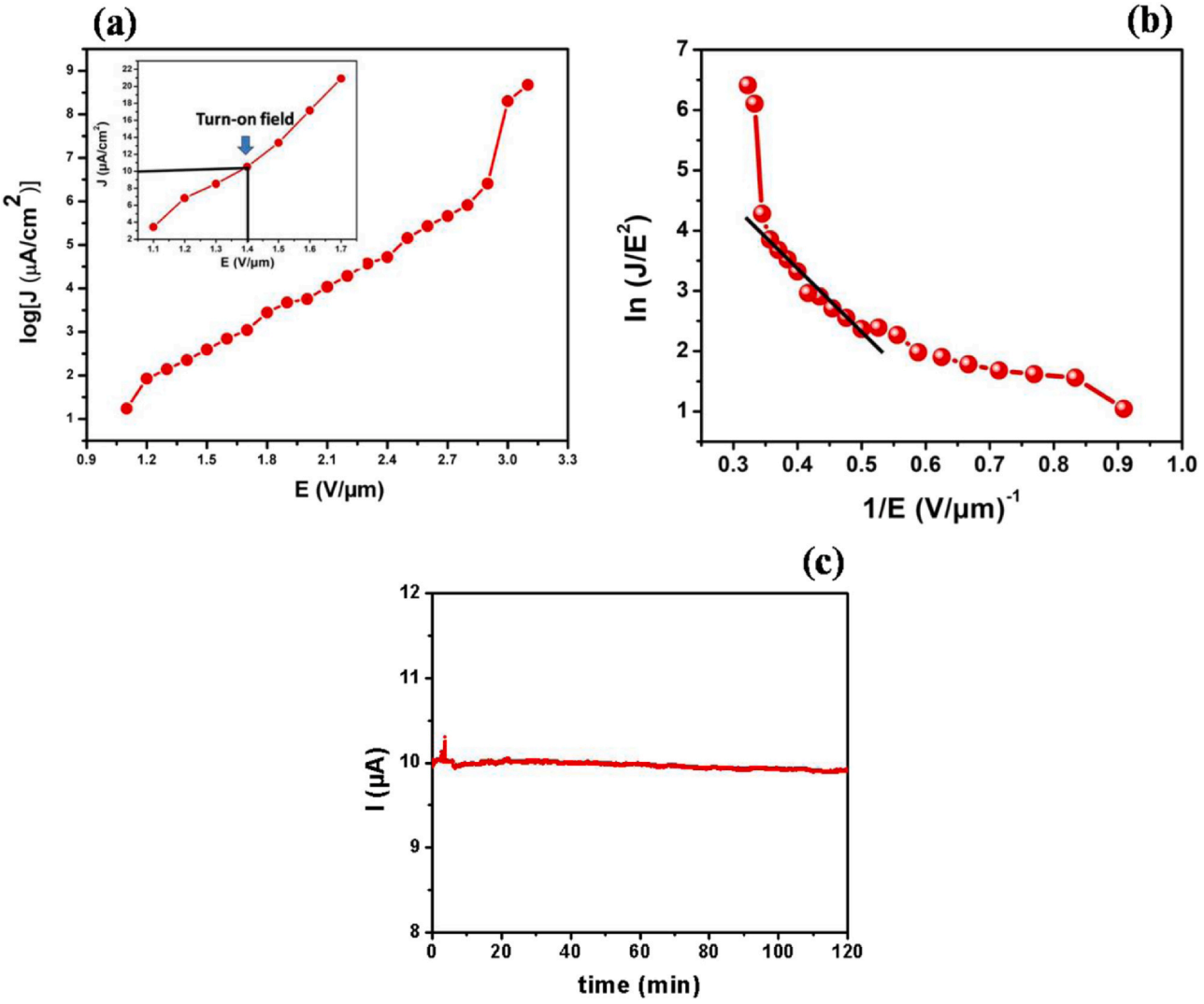

Fig. 4. (a) Log of current density vs applied field (log(*J*)-*E*) plot, (b)Fowler–Nordheim (*F*-*N*) plot and (c) emission current stability (*I*-*t*) plot recorded at 10 μA (applied voltage of 2 kV) for 2 h.

Table 1
Comparison of turn-on field with reported selenium based nanomaterials (for anode-cathode distance d =1 mm).

Sr. no.	Materials	Turn-on field (V/μm) (for J = 10 μA/cm^2)	References
1	CdSe nanotubes	1.7	[45]
2	In_2Se_3 micro-crystals	~3.40	[46]
3	In_2Se_3nanocubes	~5.8	[47]
4	In_2Se_3 nanowires	3.40	[48]
5	$PbBi_2Se_4$ nanosheets	~4.80 (1 μA/cm^2)	[49]
6	$MoSe_2$ nanoflakes	2.4 (1 μA/cm^2)	[50]
7	layered VSe_2	~3.25 (1 μA/cm^2)	[51]
8	layered $MoSe_2$	~2.3	[52]
9	SnSe nanosheets	2.25	[29]
10	CuSe nanosheets	1.4	Present work

3.2. Surface morphological properties

FESEM analysis confirms the surface topography of the CuSe nanosheets as shown in Fig. 2(b–d). The high magnification image showed in Fig. 2b reveals a large coverage of nanosheets and a close up image in Fig. 2c shows vertically aligned nanosheets of CuSe. The average thickness of the nanosheets is about 34 nm with the average lateral size estimated at 700 nm (Fig. 2c). TEM characterization (Fig. 3a) further confirms the 2D nanosheet-like morphology of CuSe. The HRTEM image in Fig. 3b reveals the single crystalline nature of CuSe with fringe spacing of 0.34 nm [44]. The inset of Fig. 3b is the SAED pattern, which confirms that the sample is single crystalline. The SAED pattern recorded perpendicular to the (001) surface that could be attributed to the [001] zone-axis diffraction of the hexagonal phase of CuSe. The fuzzy spots may be due to the line defect and overlapping of CuSe nanosheets. The bright TEM image (Fig. 3c) is employed for elemental mapping analysis, which shows an equal distribution of C, Cu and Se elements throughout the 2D CuSe nanosheet as shown in Fig. 3(d–f).

3.3. Field emission studies

The field emission properties of the vertically aligned 2D single crystalline CuSe nanosheets have been expounded by the way of log of current density versus applied field (log(*J*)-*E*), Fowler–Nordheim (*F*-*N*) and emission current stability versus time (*I*-*t*) plots. The turn-on field, defined in the present study as the minimum field required to withdraw an emission current of 10 μA/cm^2 is found to be 1.4 V/μm (inset of Fig. 4a). The maximum current density withdrawn from the emitter material is observed to be 5.8 mA/cm^2 at an applied electric field of 3.1 V/μm. Table 1 shows the comparison between the turn-on field values of selenium based nanomaterials and the vertically aligned 2D CuSe nanosheets [45–52,29]. The field enhancement factor (β) [53] has

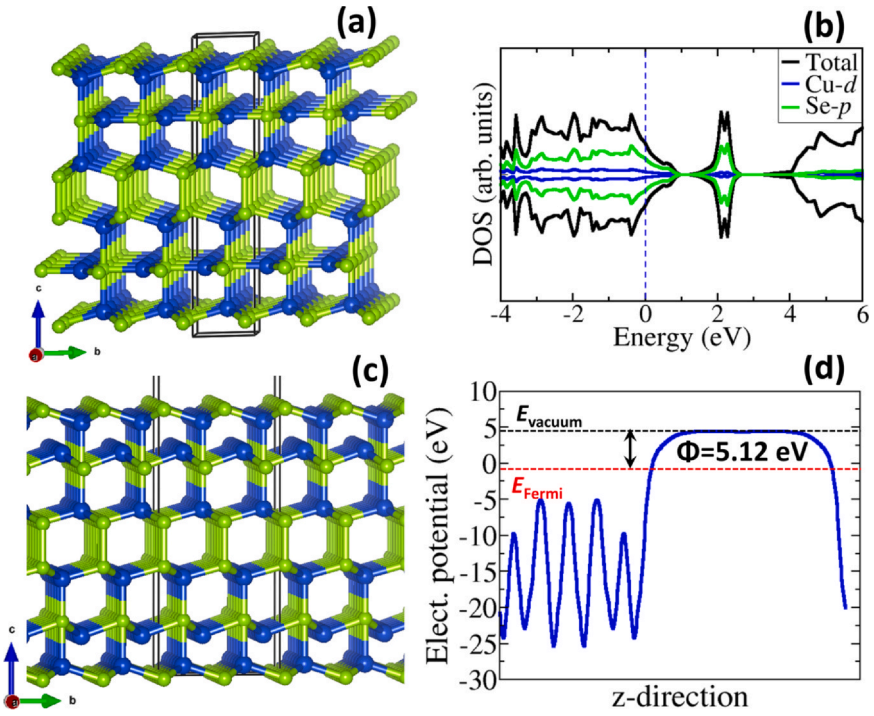

Fig. 5. (a) Crystal structure of CuSe, (b) the partial density of states (PDOS), (c) the optimized CuSe(001) surface in the side view and (d) the corresponding electrostatic potentials for the CuSe(001) surface. The black and red dashed lines represent the vacuum level (E_{vacuum}) and the Fermi level (E_{Fermi}), respectively. The Φ is the work function. (For interpretation of the references to color in this figure legend, the reader is referred to the web version of this article.)

been calculated by using an *F-N* plot based on the formula: $\beta = \frac{-(6.8 \times 10^3)\phi^{\frac{3}{2}}}{\text{slope}}$, where, ϕ is work function. The value of β is calculated at 3545. The overall nature of observed F-N plot is seen to be non-linear. For the calculation of β, higher field region of F-N plot has been chosen and it is shown in Fig. 4b. Possible reasons behind the observed impressive field emission characteristics are suggested to be due to the sharp edges, vertically aligned morphology, high β value and the metallic nature of CuSe [28]. According to SAED indexing and owing to the stability of the (001) surface, it is expected to be the most expressed and abundant facet in CuSe nanocrystals. Thus, the field emission is suggested to come from the most stable and most expressed (001) surface. The vertically aligned 2D CuSe nanosheets display a quite stable emission current (10 μA at 2 kV) recorded over a 2 h period of testing (Fig. 4c). As the field emission is a surface sensitive phenomenon, the small fluctuations observed in *I-t* plot during initial period of measurement may be credited to the adsorption/desorption of residual gases [29].

3.4. Density functional theory (DFT)

In view of the fact that field emission characteristics are dependent on the work function (Φ) of the emissive material, we have carried out electronic structure calculations based on density functional theory (DFT) to gain atomic-level insight into the electronic structure and work function of CuSe. The bulk klockmannite CuSe was modeled in the hexagonal crystal structure (space group – $P6_3/mmc$) [54,55] as shown in Fig. 5a. The (001) surface is also predicted to be the most stable for CuSe, which is isostructural to CuS. Therefore, the CuSe (001) surface is chosen for the DFT calculations. The fully relaxed unit cell parameters were predicted at $a = 3.980$ Å and $c = 17.259$ Å, which compares closely with experimental data and previous theoretical structure of hexagonal CuSe [54,55]. The metallic characteristic of CuSe [56] is also well reproduced, as shown by the electronic projected density of states (PDOS) in Fig. 5b, with the Se atoms contributing a higher proportion of density of states at the Fermi level than Cu atoms. This is consistent with the metallic behavior exhibited by the isostructural covellite CuS [57]. The optimized structure of the CuSe(001) surface employed to characterize the work function is shown Fig. 5c, with the corresponding electrostatic potential shown in Fig. 5d. The work function of the CuSe(001) surface is 5.12 eV versus vacuum. The gas molecules that may adsorb on the sample surface during field emission experiments, could further decreases the work function owing to the adsorption induced electron density redistribution in the gas-covered sample surfaces [57]. As the work function dictates the electron emission capability of a the emitter material, the low work function calculated for the CuSe(001) is suggested as the primary origin for the impressive field electron emission characteristics observed in Fig. 4.

4. Conclusion

In summary, we have employed a non-hazardous, economical and simple technique for synthesis of vertically aligned single crystalline CuSe nanosheets. The 2D CuSe nanosheets are demonstrated to show impressive turn-on field of 1.4 V/μm for 10 μA/cm^2 emission current density and a high emission current density of 5.8 mA/cm^2 at an applied electric field of 3.1 V/μm. The CuSe nanomaterials exhibit metallic conductivity and a low work function of 5.12 eV for the CuSe(001) surface as predicted from first-principles DFT calculations. The observed excellent field emission characteristics of single crystalline CuSe nanosheets may be due to sharp edges, vertically aligned nature, high β value, metallic conductivity, and low work function. Our results show that the controlled synthesis of 2D CuSe nanosheets may open new avenues for further development towards efficient field emission applications.

CRediT authorship contribution statement

Chandradip D. Jadhav and Sachin R. Rondiya: performed synthesis, field emission studies, characterizations, and wrote manuscript. **Padmakar G. Chavan**: contributed to the study design and scientific discussions on methods and conclusions. **Nelson Y.**

Dzade and Sachin R. Rondiya: carried out the DFT simulations and data analysis. **Reshma C. Hambire, Devshri R. Baviskar and Avinash V. Deore**: supported during synthesis and analysis. **Russell W. Cross:** supported computational studies.

Declaration of Competing Interest

The authors declare that they have no known competing financial interests or personal relationships that could have appeared to influence the work reported in this paper.

Acknowledgements

C.D.J. and P.G.C. would like to thank Dr. Bidhan Pandit and Dr. Khemchand Dewangan for providing TEM characterization facility and for fruitful discussion regarding TEM. P.G.C. also thanks the Consortium for Scientific Research (CSR) Indore, India for financial support (CSR project - CSR-IC-MSRSR-19/CRS-227/2017–2018/1308).S.R.R., R.W.C., and N.Y.D. acknowledge the UK Engineering and Physical Sciences Research Council (EPSRC) for funding (Grant No. EP/S001395/1). This work has also used the computational facilities of the Advanced Research Computing at Cardiff (ARCCA) Division, Cardiff University, and HPC Wales. This work also made use of the facilities of ARCHER (http://www.archer.ac.uk), the UK's national supercomputing service via the membership of the UK's HEC Materials Chemistry Consortium, which is funded by EPSRC (EP/L000202). Information on the data that underpins the results presented here, including how to access them, can be found in the Cardiff University data catalogue at http://doi.org/10.17035/d.2021.0133742344.

References

[1] H.-C. Xia, Y. Xia, X. Peng, Shape-controlled synthesis of colloidal metal nanocrystals: thermodynamic versus kinetic products, J. Am. Chem. Soc. 137 (2015) 7947–7966.
[2] V.I. Klimov, Semiconductor and Metal Nanocrystals: Synthesis and Electronic and Optical Properties, CRC Press, New York, 2003.
[3] A. Sun, S. Murray, C.B. Weller, D. Folks, L. Moser, Monodisperse FePt nanoparticles and ferromagnetic FePt nanocrystal superlattices, Science 287 (2000) 1989–1992.
[4] C.Y. Gong Y, H. Yuan, C.L. Wu, P. Tang, S.Z. Yang, A. Yang, G. Li, B. Liu, J. van de Groep, M.L. Brongersma, M.F. Chisholm, S.C. Zhang, W. Zhou, Spatially controlled doping of two-dimensional SnS2 through intercalation for electronics, Nat. Nanotechnol. 13 (2018) 294–299.
[5] L.& L. Wu, G. Chan, K.C. Zhu, L. Sun, Dual-phase nanostructuring as a route to high-strength magnesium alloys, Nature 545 (2017) 80–83.
[6] M. Asadi, K. Kim, C. Liu, A.V. Addepalli, P. Abbasi, P. Yasaei, P. Phillips, A. Behranginia, J.M. Cerrato, R. Haasch, P. Zapol, B. Kumar, R.F. Klie, J. Abiade, L.A. Curtiss, A. Salehi-Khojin, Nanostructured transition metal dichalcogenide electrocatalysts for CO_2 reduction in ionic liquid, Science 353 (2016) 467–470, https://doi.org/10.1126/science.aaf4767
[7] A.-Y. Lu, H. Zhu, J. Xiao, C.-P. Chuu, Y. Han, M.-H. Chiu, C.-C. Cheng, C.-W. Yang, K.-H. Wei, Y. Yang, Y. Wang, D. Sokaras, D. Nordlund, P. Yang, D.A. Muller, M.-Y. Chou, X. Zhang, L.-J. Li, Janus monolayers of transition metal dichalcogenides, Nat. Nanotechnol. 12 (2017) 744–749, https://doi.org/10.1038/nnano.2017.100
[8] S. Deka, A. Genovese, Y. Zhang, K. Miszta, G. Bertoni, R. Krahne, C. Giannini, L. Manna, Phosphine-free synthesis of p-type copper(I) selenide nanocrystals in hot coordinating solvents, J. Am. Chem. Soc. 132 (2010) 8912–8914, https://doi.org/10.1021/ja103223x
[9] J. Xu, C.-S. Lee, Y.-B. Tang, X. Chen, Z.-H. Chen, W.-J. Zhang, S.-T. Lee, W. Zhang, Z. Yang, Large-scale synthesis and phase transformation of CuSe, $CuInSe_2$, and $CuInSe_2$/$CuInS_2$ core/shell nanowire bundles, ACS Nano 4 (2010) 1845–1850, https://doi.org/10.1021/nn9013627
[10] G.B. Sakr, I.S. Yahia, M. Fadel, S.S. Fouad, N. Romčević, Optical spectroscopy, optical conductivity, dielectric properties and new methods for determining the gap states of CuSe thin films, J. Alloy. Compd. 507 (2010) 557–562, https://doi.org/10.1016/j.jallcom.2010.08.022
[11] A. Abraham, Tarachand, G.S. Okram, R. Jacob, P.V. Sreenivasan, R.R. Philip, Low temperature electrical conductivity and seebeck coefficient of nanostructured CuSe thin films with Ga addition, Vacuum 129 (2016) 74–78, https://doi.org/10.1016/j.vacuum.2016.04.011
[12] M. Senthilkumar, M. CI, B. SM, Morphological controlled synthesis of hierarchical copper selenide nanocrystals by oleic acid, 1-dodecanethiol and 1-octadecene as surfactants, J. Cryst. Growth 468 (2017) 169–174, https://doi.org/10.1016/j.jcrysgro.2016.11.001
[13] C.-T. Yang, H.-I. Hsiang, J.-H. Tu, Copper selenide crystallites synthesized using the hot-injection process, Adv. Powder Technol. 27 (2016) 959–963, https://doi.org/10.1016/j.apt.2016.03.004
[14] X. Hou, P. Xie, S. Xue, H. Feng, L. Li, Z. Liu, R. Zou, The study of morphology-controlled synthesis and the optical properties of CuSe nanoplates based on the hydrothermal method, Mater. Sci. Semicond. Process. 79 (2018) 92–98, https://doi.org/10.1016/j.mssp.2018.01.023
[15] X. Chen, Z. Li, J. Yang, Q. Sun, S. Dou, Aqueous preparation of surfactant-free copper selenide nanowires, J. Colloid Interface Sci. 442 (2015) 140–146, https://doi.org/10.1016/j.jcis.2014.11.052
[16] Y. Chen, D. Wang, Y. Lin, X. Zou, T. Xie, In suit growth of CuSe nanoparticles on MXene (Ti_3C_2) nanosheets as an efficient counter electrode for quantum dot-sensitized solar cells, Electrochim. Acta 316 (2019) 248–256, https://doi.org/10.1016/j.electacta.2019.05.132
[17] Z.H. Han, Y.P. Li, H.Q. Zhao, S.H. Yu, X.L. Yin, Y.T. Qian, A simple solvothermal route to copper chalcogenides, Mater. Lett. 44 (2000) 366–369, https://doi.org/10.1016/S0167-577X(00)00060-4
[18] S. Muthu, M. Babu Sridharan, Synthesis and characterization of two dimensional copper selenide (CuSe) Nanosheets, Mater. Today Proc. 5 (2018) 23161–23168, https://doi.org/10.1016/j.matpr.2018.11.047
[19] Y.-Q. Liu, F.-X. Wang, Y. Xiao, H.-D. Peng, H.-J. Zhong, Z.-H. Liu, G.-B. Pan, Facile microwave-assisted synthesis of klockmannite CuSe nanosheets and their exceptional electrical properties, Sci. Rep. 4 (2014) 5998, https://doi.org/10.1038/srep05998
[20] Y. An, Y. Hou, H. Wang, J. Li, R. Wu, C. Liu, T. Wang, J. Jiao, Multifunctional 2D CuSe monolayer nanodevice, J. Phys. Condens. Matter 31 (2019) 355301, https://doi.org/10.1088/1361-648X/ab18e5
[21] S. Yang, F. Ji, Z. Wang, Y. Zhu, K. Hu, Y. Ouyang, R. Wang, X. Ma, C. Cao, Microwave-assisted synthesis of CuSe nano-particles as a high -performance cathode for rechargeable magnesium batteries, Electrochim. Acta 324 (2019) 134864, https://doi.org/10.1016/j.electacta.2019.134864
[22] S.R. Alharbi, A.F. Qasrawi, Structural and optoelectronic properties of MoO_3/CuSe interfaces, Phys. Status Solidi A 216 (2019) 1800977, https://doi.org/10.1002/pssa.201800977
[23] R. Zou, Z. Zhang, Q. Liu, K. Xu, G. He, J. Hu, A facile approach for the synthesis of Cu2-x Se nanowires and their field emission properties, J. Mater. Sci. 49 (2014) 532–537, https://doi.org/10.1007/s10853-013-7731-9
[24] C.D. Jadhav, S.S. Karade, B.R. Sankapal, G.P. Patil, P.G. Chavan, Reduced turn-on field through solution processed MoS_2 nanoflakes anchored MWCNTs, Chem. Phys. Lett. 723 (2019) 146–150, https://doi.org/10.1016/j.cplett.2019.03.035
[25] V.S. Bagal, G.P. Patil, C. Jadhav, M. Sharma, S. Shivhare, P.G. Chavan, Field electron extraction from surface modified Cd(OH)2 nanowires, AIP Conf. Proc. 1942 (2018) 50032, https://doi.org/10.1063/1.5028663
[26] A. Datta, P.G. Chavan, F.J. Sheini, M.A. More, D.S. Joag, A. Patra, Growth, optical, and field emission properties of aligned CdS nanowires, Cryst. Growth Des. 9 (2009) 4157–4162, https://doi.org/10.1021/cg900388v
[27] V.S. Bagal, G.P. Patil, A.B. Deore, P.K. Baviskar, S.R. Suryawanshi, M.A. More, P.G. Chavan, High current density and low turn-on field from aligned $Cd(OH)_2$ nanosheets, Chem. Phys. Lett. 650 (2016) 7–10, https://doi.org/10.1016/j.cplett.2016.02.052
[28] C.D. Jadhav, B. Pandit, S.S. Karade, B.R. Sankapal, P.G. Chavan, Enhanced field emission properties of V_2O_5/MWCNTs nanocomposite, Appl. Phys. A 124 (2018) 794, https://doi.org/10.1007/s00339-018-2218-9
[29] S.R. Rondiya, C.D. Jadhav, P.G. Chavan, N.Y. Dzade, Enhanced field emission properties of Au/SnSe nano-heterostructure: a combined experimental and theoretical investigation, Sci. Rep. 10 (2020) 2358, https://doi.org/10.1038/s41598-020-58840-8
[30] G.P. Patil, P.K. Baviskar, V.S. Bagal, R.D. Ladhe, A.B. Deore, M.A. More, B.R. Sankapal, P.G. Chavan, Aligned 2D CuSCN nanosheets: a high performance field emitter, RSC Adv. 6 (2016) 71958–71962, https://doi.org/10.1039/C6RA16013A
[31] V.S. Bagal, G.P. Patil, A.B. Deore, P.K. Baviskar, D.J. Shirale, P.G. Chavan, Enhanced field emission properties from surface-modified 2D $Cd(OH)_2$ nanocoins, Appl. Phys. A 123 (2017) 125, https://doi.org/10.1007/s00339-016-0741-0
[32] S.R. Rondiya, I. Karbhal, C.D. Jadhav, M.P. Nasane, T.E. Davies, M.V. Shelke, S.R. Jadkar, P.G. Chavan, N.Y. Dzade, Uncovering the origin of enhanced field emission properties of rGO–MnO2 heterostructures: a synergistic experimental and computational investigation, RSC Adv. 10 (2020) 25988–25998, https://doi.org/10.1039/D0RA03360J
[33] Hendrik J. Monkhorst, James D. Pack, Special points for Brillonin-zone integrations, J. Mater. Chem. A 7 (2019) 2156–2164, https://doi.org/10.1039/c8ta11250a
[34] J.P. Perdew, K. Burke, M. Ernzerhof, Generalized gradient approximation made simple, Phys. Rev. Lett. 78 (1997) 1396, https://doi.org/10.1103/PhysRevLett.77.3865
[35] A.V. Krukau, O.A. Vydrov, A.F. Izmaylov, G.E. Scuseria, Influence of the exchange screening parameter on the performance of screened hybrid functionals, J. Chem. Phys. 125 (2006) 224106, https://doi.org/10.1063/1.2404663
[36] P.E. Blöchl, Projector augmented-wave method, Phys. Rev. B 50 (1994) 17953–17979, https://doi.org/10.1103/PhysRevB.50.17953
[37] Á. Morales-García, J. He, A.L. Soares, H.A. Duarte, Surfaces and morphologies of covellite (CuS) nanoparticles by means of: ab initio atomistic thermodynamics, CrystEngComm 19 (2017) 3078–3084, https://doi.org/10.1039/c7ce00203c
[38] R. Gaspari, L. Manna, A. Cavalli, A theoretical investigation of the (0001) covellite surfaces, J. Chem. Phys. 141 (2014) 044702, https://doi.org/10.1063/1.4890374
[39] A. Walsh, K.T. Butler, Prediction of electron energies in metal oxides, Acc. Chem. Res. 47 (2014) 364–372, https://doi.org/10.1021/ar400115x

[40] A.M. Ganose, K.T. Butler, A. Walsh, D.O. Scanlon, Relativistic electronic structure and band alignment of BiSI and BiSeI: candidate photovoltaic materials, J. Mater. Chem. A 4 (2016) 2060–2068, https://doi.org/10.1039/c5ta09612j
[41] L. Wu, N.Y. Dzade, L. Gao, D.O. Scanlon, Z. Öztürk, N. Hollingsworth, B.M. Weckhuysen, E.J.M. Hensen, N.H. de Leeuw, J.P. Hofmann, Enhanced photoresponse of FeS_2 films: the role of marcasite–pyrite phase junctions, Adv. Mater. 28 (2016) 9602–9607, https://doi.org/10.1002/adma.201602222
[42] Reen, United States Patent, 1976.
[43] M. Tsujikawa, D. Yoshida, N. Yamauchi, N. Ueda, T. Sone, Surface modification of SUS304 stainless steel using carbon push-ahead effect by low temperature plasma nitriding, Mater. Trans. 46 (2005) 863–868, https://doi.org/10.2320/matertrans.46.863
[44] L. Tan, Z.Q. Liu, N. Li, J.Y. Zhang, L. Zhang, S. Chen, CuSe decorated carbon nanotubes as a high performance cathode catalyst for microbial fuel cells, Electrochim. Acta 213 (2016) 283–290, https://doi.org/10.1016/j.electacta.2016.07.099
[45] P.G. Patil, P. Girish, Baviskar, K. Prashant, Chavan, Ultra low turn-on and photosensitive field emission from CdSe nanotubes, J. Nanoelectron. Optoelectron. 14 (2019) 470–474.
[46] Z. Gao, S. Xue, Q. Yu, P. Xie, Y. Wang, H. Feng, L. Li, Synthesis, field emission of various ZnSe nanostructures by hydrothermal methods, Micro Nano Lett. 12 (2017) 382–385, https://doi.org/10.1049/mnl.2016.0808
[47] G. Li, T. Zhai, Y. Jiang, Y. Bando, D. Golberg, Enhanced field-emission and red lasing of ordered CdSe nanowire branched arrays, J. Phys. Chem. C 115 (2011) 9740–9745, https://doi.org/10.1021/jp200398s
[48] Q. Su, L. Li, S. Li, H. Zhao, Field-emission property of ZnSe nanoarrays, Micro Nano Lett. 7 (2012) 1053–1055, https://doi.org/10.1049/mnl.2012.0589
[49] Y. Zhang, H. Li, L. Jiang, H. Liu, C. Shu, Y. Li, C. Wang, Field emission from GeSe2 nanowalls, Appl. Phys. Lett. 98 (2011) 113118, https://doi.org/10.1063/1.3569147
[50] L. Zhao, Q. Pang, Y. Cai, N. Wang, W. Ge, J. Wang, S. Yang, Vertically aligned zinc selenide nanoribbon arrays: microstructure and field emission, J. Phys. D Appl. Phys. 40 (2007) 3587–3591, https://doi.org/10.1088/0022-3727/40/12/007
[51] L. Zhao, Q. Pang, S. Yang, W. Ge, J. Wang, Realization and field emission of CdSe nano-tetrapods with different arm lengths, Phys. Lett. Sect. A Gen. Solid State Phys. 373 (2009) 2965–2968, https://doi.org/10.1016/j.physleta.2009.06.032
[52] S.X. n Weikang Zhou, P.X. Junwei Han, Synthesis of grass-like ZnSe nanostructures on graphene oxide and their excellent field emission properties, Mater. Lett. 134 (2014) 256–258.
[53] K.J. Sankaran, D.Q. Hoang, S. Kunuku, S. Korneychuk, S. Turner, P. Pobedinskas, S. Drijkoningen, M.K. Van Bael, J. D'Haen, J. Verbeeck, K.C. Leou, I.N. Lin, K. Haenen, Enhanced optoelectronic performances of vertically aligned hexagonal boron nitride nanowalls-nanocrystalline diamond heterostructures, Sci. Rep. 6 (2016) 1–11, https://doi.org/10.1038/srep29444
[54] J.W. Earley, Studies of natural and artificial selenides: I—Klockmannite, CuSe*, Am. Mineral. 34 (1949) 435–440.
[55] L.G. Berry, The crystal structure of covellite, cuse and klockmannite, cuse, Am. Mineral. 39 (1954) 504–509.
[56] V. Milman, Klockmannite, CuSe: structure, properties and phase stability from ab initio modeling, Acta Crystallogr. Sect. B Struct. Sci. 58 (2002) 437–447, https://doi.org/10.1107/S0108768102003269
[57] A. Morales-García, A.L. Soares, E.C. Dos Santos, H.A. De Abreu, H.A. Duarte, First-principles calculations and electron density topological analysis of covellite (CuS), J. Phys. Chem. A 118 (2014) 5823–5831, https://doi.org/10.1021/jp4114706